Available online at www.sciencedirect.com

ScienceDirect

IFAC Papers Online CONFERENCE PAPER ARCHIVE

IFAC PapersOnLine 53-2 (2020) 14827–14832

Nonlinear Dynamic Inversion Autopilot Design for Dual-Spin Guided Projectiles

Steven Tipán * **Sovanna Thai** * **Michael Proff** *
Spilios Theodoulis *

* *Department of Guidance, Navigation and Control, French-German Research Institute of Saint-Louis, 5 rue du Général Cassagnou, 68301, Saint-Louis, FR (Spilios.Theodoulis@isl.eu).*

Abstract: This paper deals with the autopilot design for a 155-mm dual-spin projectile equipped with a course correction fuze (CCF). This class of projectiles is subject to high nonlinearities and to strongly coupled dynamics between its pitch and yaw channels. To overcome these difficulties a Nonlinear Dynamic Inversion (NDI) based autopilot is proposed. This autopilot possesses a cascade structure where an inner loop linearises the nonlinear system dynamics and an outer loop enables to impose the desired system closed-loop dynamics. The configuration of a dual-spin projectile requires the development of two separate control loops, one for the roll channel and another for the pitch/yaw channels. The pitch/yaw controller is developed under a Time Scale Separation (TSS) scheme. This not only helps to accelerate the design of the control laws but also to achieve a satisfactory level of robustness. The autopilots are also validated with a nonlinear 7-DOF simulation.

Copyright © 2020 The Authors. This is an open access article under the CC BY-NC-ND license (http://creativecommons.org/licenses/by-nc-nd/4.0)

Keywords: Nonlinear Dynamic Inversion, Time Scale Separation, Guided projectiles.

1. INTRODUCTION

Standard artillery shells lack precision being essentially non-guided weapons following a ballistic trajectory. The result is poor performance in the presence of incorrect launch parameters or external disturbances and cost increase due to the high number of firing rounds required to hit a target. The requirements for this type of ammunition increasingly demand an improvement in accuracy and range in order to avoid any undesired outcome on the battlefield. Therefore, the development of guided projectiles has become an important field of research in recent years.

Various mechanisms have been proposed to correct the trajectory of a projectile during flight, for example, jet thrusters (Davis et al. (2009)) or aerodynamic control surfaces (Fresconi et al. (2012); Theodoulis and Wernert (2017)). The latter solution presents various advantages, for instance, it can provide with continuous control over the projectile and its physical fundamentals are well-known. In addition, a projectile equipped with control surfaces presents with similarities with respect to missiles, hence easing the development of a control system.

The nose-located guidance module contains all necessary hardware (sensors, actuators, etc.) and provides with all the commands necessary to correct the trajectory and hit a target. The control system itself guarantees closed-loop stability and makes the system track acceleration commands in a rapid and stable way.

Previous work for guided projectile control system design was mainly based on linear control theory, requiring to develop multivariable robust control laws and apply gain-scheduling techniques (Theodoulis et al. (2013, 2015); Sève et al. (2017b)).

The overall design process is hence time-consuming since performance and robustness properties must be checked for a large number of operating points. A dual-spin guided projectile is characterized by strongly nonlinear dynamics and therefore a natural approach to address the control design problem is via a purely nonlinear controller. Such an approach allows for rapid control law prototyping since just a single (nonlinear) controller would be valid over the whole flight envelope. Still, relatively few works based on nonlinear control theory for these systems exist (Lee et al. (2014); Yuanchuan et al. (2017); Sung et al. (2019)).

This paper proposes a Nonlinear Dynamic Inversion (NDI)-based controller for the autopilot design. NDI is a multivariable control technique, widely used in industry, that follows a rather straightforward design procedure. It is necessary to develop only one (nonlinear) controller for the whole flight envelope, thus avoiding the need for any gain-scheduling. Besides, the use of NDI allows for the desired closed-loop dynamics of the system to be established directly during controller design. Examples in the literature where NDI was successfully implemented may be found, from missiles to re-entry aerospace vehicles (Menon and Yousefpor (1996); da Costa et al. (2003)). Despite its obvious advantages, an NDI controller presents some drawbacks, usually its lack of robustness. This is here addressed through a Time Scale Separation (TSS) scheme, helping to simplify the developed control law but also to improve the system robustness (Menon et al. (1997)).

The paper is organized as follows: Section 2 presents the 7-DOF nonlinear model for the projectile dynamics, Section 3 addresses the autopilot design for both the roll channel and pitch/yaw channels, and Section 4 provides with the nonlinear simulation results for validation.

2405-8963 © 2020, IFAC (International Federation of Automatic Control) Hosting by Elsevier Ltd. All rights reserved.
Peer review under responsibility of International Federation of Automatic Control.
10.1016/j.ifacol.2020.12.1926

2. AIRFRAME MODELING

This section shortly presents the dual-spin projectile configuration and the underlying nonlinear flight dynamics equations required for control design.

2.1 System Concept

The development of a new guided projectile system is usually quite a long process that implies a high cost. For this reason, a more intelligent approach followed to develop guided projectiles while maintaining a low-cost development is to modify existing ballistic projectiles and convert them into guided weapons. This project is conducted under this context, where a 155mm spin-stabilized projectile is modified to integrate a Roll-Decouple Course Correction Fuze (CCF) (Theodoulis and Wernert (2017)). The resulting configuration is known as a dual-spin projectile (Costello and Peterson (2000)) and allows for the use of existing ammunition, thus helping to reduce production costs. The overall structure consists of two parts, the main body, which spins at a high rate in order to guarantee the stability of the system, and a forward part or fuze where the various control surfaces are integrated. These more precisely consist of a pair of rotating canards, which make possible to aerodynamically control the roll and pitch/yaw (lateral) channels.

2.2 Nonlinear Mathematical Model

The projectile equations of motion are traditionally written using a specific Body-Fixed Roll (BFR) frame (Wernert et al. (2010)). Using a conventional frame B that would roll along with the body presents some drawbacks for a spin-stabilized projectile. Due to the high body spin rate (around 250Hz), the simulation step would have to be small enough to capture its roll dynamics. This ultimately results in a total simulation time which can be quite long and also the accumulated numerical errors may be larger.

A BFR reference frame though is characterized by not experiencing a roll motion and helps to overcome the above issues. The details on how the nonlinear flight dynamics equations can be written using such a reference frame are omitted but can be found in Sève et al. (2017a).

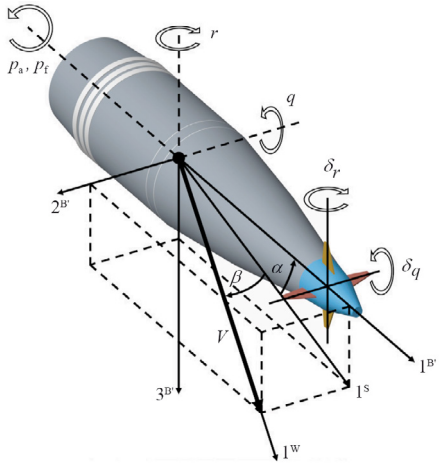

Fig. 1. Dual-spin projectile concept.

For control design purposes, it is more convenient to use as states the variables (V, α, β) instead of the linear velocities (u, v, w). Therefore, assuming no wind disturbances and by performing appropriate transformations, the 7DoF translational and angular nonlinear flight dynamics equations can be represented as (for more details refer to Sève et al. (2017a)):

$$\begin{bmatrix}\dot{V}\\ \dot{\alpha}\\ \dot{\beta}\end{bmatrix} = \begin{bmatrix}0\\ q + r(\cos\alpha\tan\theta - \sin\alpha)\tan\beta\\ -r(\cos\alpha + \sin\alpha\tan\theta)\end{bmatrix} + \left(\frac{1}{mV}\right)\begin{bmatrix}V\cos\alpha\cos\beta & V\sin\beta & V\sin\alpha\cos\beta\\ -\sin\alpha/\cos\beta & 0 & \cos\alpha/\cos\beta\\ -\cos\alpha\sin\beta & \cos\beta & -\sin\alpha\sin\beta\end{bmatrix}\begin{bmatrix}X\\ Y\\ Z\end{bmatrix} \tag{1}$$

$$\begin{bmatrix}\dot{p}_f\\ \dot{p}_a\\ \dot{q}\\ \dot{r}\end{bmatrix} = \begin{bmatrix}0\\ 0\\ -r(r\tan\theta + I_{xx,a}I_{yy}^{-1}p_a)\\ q(r\tan\theta + I_{xx,a}I_{zz}^{-1}p_a)\end{bmatrix} + \begin{bmatrix}L_f/I_{xx,f}\\ L_a/I_{xx,a}\\ M/I_{yy}\\ N/I_{zz}\end{bmatrix} \tag{2}$$

The externally-applied forces to the projectile can be written as:

$$\begin{aligned}\begin{bmatrix}X\\ Y\\ Z\end{bmatrix} &= \begin{bmatrix}X_B\\ Y_B\\ Y_B\end{bmatrix} + \begin{bmatrix}X_C\\ Y_C\\ Y_C\end{bmatrix} + \begin{bmatrix}X_M\\ Y_M\\ Y_M\end{bmatrix} + \begin{bmatrix}X_G\\ Y_G\\ Y_G\end{bmatrix}\\ &= \bar{q}S\left(\begin{bmatrix}-C_A\\ C_{Y\beta}\beta\\ -C_{N\alpha}\alpha\end{bmatrix} + \begin{bmatrix}0\\ C_{Y\delta}\delta_r\\ -C_{N\delta}\delta_q\end{bmatrix} + \left(\frac{p_a d}{2V}\right)\begin{bmatrix}0\\ C_{Yp\alpha}\alpha\\ -C_{Yp\alpha}\beta\end{bmatrix}\right) + mg\begin{bmatrix}-\sin\theta\\ 0\\ \cos\theta\end{bmatrix}\end{aligned} \tag{3}$$

The forces are distinguished by their aerodynamic and gravitational (G) contributions. The aerodynamic forces can be represented in terms of: body effects due to lift/drag (B), control surfaces (C) and Magnus effect (M).

The aerodynamic moments acting on the guided projectile can be also represented as a combination of similar aerodynamic effects (B), control surfaces (C), Magnus effect (M), and in addition roll/pitch/yaw damping (D) and the friction between the main body and fuse (F).

$$\begin{aligned}\begin{bmatrix}L_f\\ L_a\\ M\\ N\end{bmatrix} &= \begin{bmatrix}L_{B,f}\\ L_{B,a}\\ M_B\\ N_B\end{bmatrix} + \begin{bmatrix}L_{C,f}\\ L_{C,a}\\ M_C\\ N_C\end{bmatrix} + \begin{bmatrix}L_{M,f}\\ L_{M,a}\\ M_M\\ N_M\end{bmatrix} + \begin{bmatrix}L_{D,f}\\ L_{D,a}\\ M_D\\ N_D\end{bmatrix} + \begin{bmatrix}L_{F,f}\\ L_{F,a}\\ M_F\\ N_F\end{bmatrix}\\ &= \bar{q}Sd\left(\begin{bmatrix}0\\ 0\\ C_{m\alpha}\alpha\\ C_{n\beta}\beta\end{bmatrix} + \begin{bmatrix}C_{l\delta}\delta_p\\ 0\\ C_{m\delta}\delta_q\\ C_{n\delta}\delta_r\end{bmatrix} + \left(\frac{p_a d}{2V}\right)\begin{bmatrix}0\\ 0\\ C_{np\alpha}\beta\\ C_{np\alpha}\alpha\end{bmatrix} + \begin{bmatrix}0\\ C_{lp}p_a\\ C_{mq}q\\ C_{nr}r\end{bmatrix}\right) + \begin{bmatrix}L_{f-a}\\ -L_{f-a}\\ 0\\ 0\end{bmatrix}\end{aligned} \tag{4}$$

Given the projectile symmetry, it is possible to define that: $C_{Y\beta} = -C_{N\alpha}$, $C_{Y\delta} = C_{N\delta}$, $C_{n\beta} = -C_{m\alpha}$ and $C_{nr} = C_{mq}$.

All the above aerodynamic coefficients are usually tabulated as a function of the aerodynamic angles, Mach number, etc. whereas the dependence on the dynamic pressure $\bar{q}$ and projectile dimensions (S, d) and mass/moment of inertia also appears.

3. AUTOPILOT DESIGN

3.1 Roll Autopilot

The roll controller is used to establish a specific angular configuration for the fuze determined by the angle ϕ_f. The control is performed by the canards mounted on the fuze. First, it is necessary to present the equations which define the fuze roll dynamics:

$$\begin{bmatrix}\dot{\phi}_f \\ \dot{p}_f\end{bmatrix} = \begin{bmatrix}p_f + r\tan\theta \\ (L_{C,f} + L_{f-a})I_{xx,f}^{-1}\end{bmatrix} \tag{5}$$

where L_{f-a} is the friction moment between the forward and aft part of the projectile and is given by:

$$L_{f-a} = \overline{q}SdC_A \operatorname{sgn}(p_a - p_f)(K_s + K_v|p_a - p_f|) \tag{6}$$

The roll dynamics can be simplified since $|p_f| \gg |r\tan\theta|$:

$$\begin{bmatrix}\dot{\phi}_f \\ \dot{p}_f\end{bmatrix} = \begin{bmatrix}p_f \\ (L_{C,f} + L_{f-a})I_{xx,f}^{-1}\end{bmatrix} \tag{7}$$

It can be observed that these equations correspond to a single-input single-output (SISO) nonlinear system of second order. The output of the system is ϕ_f and the control input is δ_p. These equations can be represented in a more convenient way to apply the input-output feedback linearization method used to linearize the system.

$$\ddot{\phi}_f = (L_{C,f} + L_{f-a})I_{xx,f}^{-1} \tag{8}$$

$$y = \phi_f \tag{9}$$

The input-output feedback linearization approach requires to differentiate the output until the control input appears:

$$y = \phi_f \xrightarrow{dt} \dot{y} = \dot{\phi}_f \xrightarrow{dt} \ddot{y} = \ddot{\phi}_f = (L_{C,f} + L_{f-a})I_{xx,f}^{-1} \tag{10}$$

and hence Equation (10) can be represented as:

$$\ddot{y} = f(x) + g(x)u \tag{11}$$

where u is the control input of the system. In order to linearize the input-output map, the control input u is selected as:

$$u = \frac{1}{g(x)}[v - f(x)] \tag{12}$$

where:

$$g(x) = \overline{q}SdC_{l\delta} \tag{13}$$

$$f(x) = \overline{q}SdC_A \operatorname{sgn}(p_a - p_f)(K_s + K_v|p_a - p_f|) \tag{14}$$

Therefore, the control input $u = \delta_p$ is given by:

$$\delta_p = \frac{1}{\overline{q}SdC_{l\delta}}(v - \overline{q}SdC_A \operatorname{sgn}(p_a - p_f)(K_s + K_v|p_a - p_f|)) \tag{15}$$

Using the control signal above, the input-output map is hence linearized, and the original system becomes a chain of two integrators:

$$\ddot{y} = \ddot{\phi}_f = v \tag{16}$$

Finally, the virtual control v can be set to satisfy desired (linear) closed-loop dynamics according to design requirements. It must be underlined that the feedback linearization procedure requires the knowledge of various states of the projectile such as the roll rates p_a and p_f. Selecting v according to a PD structure gives:

$$v = K_p(\phi_c - \phi_m) - K_d\dot{\phi}_m \tag{17}$$

and the closed-loop transfer function becomes:

$$\frac{\phi_m}{\phi_c} = \frac{K_p}{s^2 + sK_d + K_p} \tag{18}$$

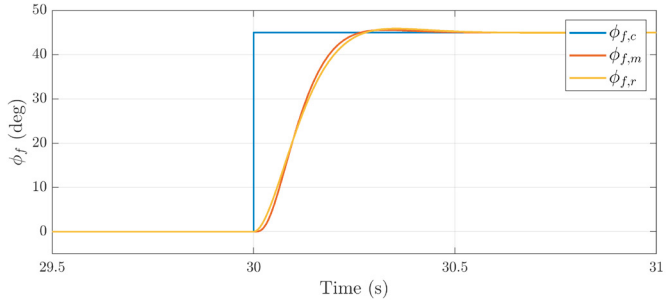

Fig. 2. Closed-loop roll angle step response.

For an ideal inversion, the system closed-loop response must correspond to this transfer function. The gains K_p, K_d can be easily computed from the equivalent second order system with $K_d = 2\xi\omega_n$ and $K_p = \omega_n^2$. Establishing an optimal damping ratio of $\xi = 0.781$ for an overshoot of 2 %, it is possible to minimize the settling time for any natural frequency. Finally, by selecting $\omega_n = 14.2$ rad/s, it is possible to obtain a settling time of $t_s = 0.25$ s. The gains of the controller using the previous values are computed as $K_d = 22.22$ and $K_p = 202.4$.

The controller is validated using a nonlinear simulation for a step response with reference amplitude of 45 deg (see Fig. 2). It can be observed that the system response is almost the same as that of the reference model. There is a relatively small delay at the beginning of the response that is a consequence of the actuator dynamics, being neglected in the design procedure for simplicity.

3.2 Lateral Autopilot

Inner Loop: The lateral (pitch-yaw) dynamics are very strongly coupled due to the very high main body spin rate, it is though possible to linearize and decouple the dynamics through NDI control by using a single controller for each channel. Due to the complexity of the equations, a TSS scheme is here employed by assuming natural time scales in the system; hence it is possible to distinguish between fast and slow dynamics. The slow dynamics relates to the body aerodynamic angles α and β whereas the fast dynamics to the body rates q and r (see Fig. 3).

Following the general control structure outlined in Fig. 3, the control design starts with the inner loop (i.e. the fast dynamics). The fast dynamics states are the body rates $[q, r]'$ and the inputs for this system are the control signals $[\delta_q, \delta_r]'$. The nonlinear design equations can be obtained from Eq. (2) by additionally considering that the products of q and r are negligible compared to the other terms. The following simplified expressions are then obtained:

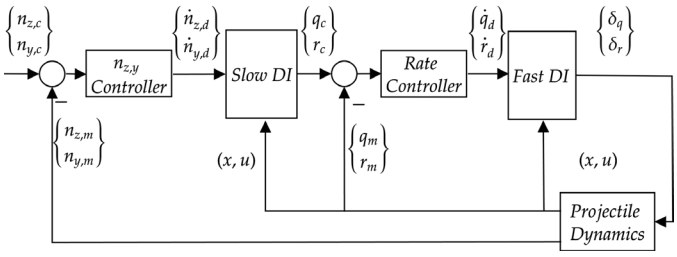

Fig. 3. NDI and TSS structure for Pitch-Yaw channels.

$$\dot{q} = -\frac{I_{xx,a}}{I_{yy}} p_a r + \frac{M}{I_{yy}} \tag{19}$$

$$\dot{r} = \frac{I_{xx,a}}{I_{zz}} p_a q + \frac{N}{I_{zz}} \tag{20}$$

Since the outputs of this system are also the body rates, these equations can be used directly when applying the input-output feedback linearization method. Using a shorthand notation, this process can be represented as:

$$y_1 = q \xrightarrow{dt} \dot{y_1} = \dot{q} = f_1(x) + g_1(x)\delta_q \tag{21}$$

$$y_2 = r \xrightarrow{dt} \dot{y_2} = \dot{r} = f_2(x) + g_2(x)\delta_r \tag{22}$$

The variables $[\dot{q}_d, \dot{r}_d]'$ represent the desired dynamics and the control commands can be then computed as:

$$\delta_{q,c} = \frac{1}{g_1(x)}[\dot{q}_d - f_1(x)] \tag{23}$$

$$\delta_{r,c} = \frac{1}{g_2(x)}[\dot{r}_d - f_2(x)] \tag{24}$$

where the functions g_1, g_2 are:

$$g_1 = \frac{\overline{q}Sd}{I_{yy}} C_{m\delta} \tag{25}$$

$$g_2 = -\frac{\overline{q}Sd}{I_{zz}} C_{m\delta} \tag{26}$$

and the functions f_1, f_2 are:

$$f_1 = \frac{\overline{q}Sd}{2I_{yy}V}(C_{mq}dq - 2I_{xx,a}Vp_a r + 2C_{m\alpha}\alpha V + C_{np\alpha}\beta p_a d) \tag{27}$$

$$f_2 = \frac{\overline{q}Sd^2}{2I_{zz}V}(C_{mq}dr + 2I_{xx,a}Vp_a q - 2C_{m\alpha}\beta V + C_{np\alpha}\alpha p_a d) \tag{28}$$

The control laws given above allow for decoupling and linearization of the projectile dynamics. The remaining control problem now is limited to properly imposing the desired inner closed-loop dynamics. This can be done using the so-called three-loop autopilot structure (Lee et al. (2014)) as:

$$\dot{q}_d = K_p \left(\frac{K_i}{s} e_q - q_m \right) \tag{29}$$

$$\dot{r}_d = K_p \left(\frac{K_i}{s} e_r - r_m \right) \tag{30}$$

where $e_q = q_c - q_m$ and $e_r = r_c - r_m$ represent the body rates errors. For an ideal inversion, $\dot{q}_m = \dot{q}_d$ and $\dot{r}_m = \dot{r}_d$ and hence the closed-loop response is computed as:

$$\frac{y_m}{y_c} = \frac{K_p K_i}{s^2 + K_p s + K_p K_i} \tag{31}$$

The inner rate controller gains are computed in a similar way as for the roll controller, with $K_p K_i = \omega_n^2$ and $K_p = 2\xi\omega_n$.

Outer Loop: Concerning the slower outer loop dynamics the simplified nonlinear equations are obtained from Eq. (1) by considering small angles and the product of small terms negligible as:

$$\dot{\alpha} = q + \frac{1}{mV} Z \tag{32}$$

$$\dot{\beta} = -r + \frac{1}{mV} Y \tag{33}$$

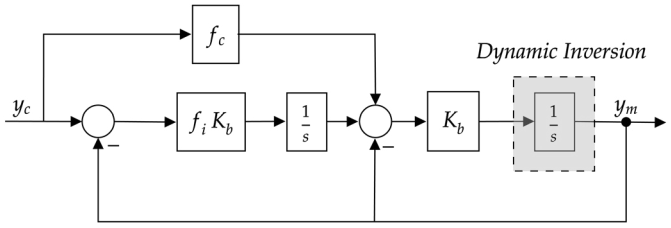

Fig. 4. Controller structure for fast dynamics control.

Before applying the feedback linearization approach, it is necessary to define the inputs of the system, which are selected to be the body rates $[q, r]'$ whereas the outputs are the normal and lateral accelerations $[n_z, n_y]'$:

$$n_z = \frac{\overline{q}S}{mg}\left[-C_{N\alpha}\alpha - \left(\frac{p_a d}{2V}\right) C_{Yp\alpha}\beta - C_{N\delta}\delta_q\right] \tag{34}$$

$$n_y = \frac{\overline{q}S}{mg}\left[C_{Y\beta}\beta + \left(\frac{p_a d}{2V}\right) C_{Yp\alpha}\alpha + C_{Y\delta}\delta_r\right] \tag{35}$$

Following the input-output feedback linearization procedure, it is necessary to differentiate the outputs until the control input appears. Using matrix notation, this process can be represented by:

$$y = \begin{bmatrix} y_1 \\ y_2 \end{bmatrix} = \begin{bmatrix} n_z \\ n_y \end{bmatrix} \xrightarrow{dt} \begin{bmatrix} \dot{y_1} \\ \dot{y_2} \end{bmatrix} = \begin{bmatrix} \dot{n}_z \\ \dot{n}_y \end{bmatrix} = \begin{bmatrix} f_{11} \\ f_{22} \end{bmatrix} + \begin{bmatrix} g_{11} & g_{12} \\ g_{21} & g_{22} \end{bmatrix} \begin{bmatrix} q \\ r \end{bmatrix} \tag{36}$$

The outputs need to be derivated only once since $\dot{\alpha}$ and $\dot{\beta}$ depend directly on the inputs $[q, r]'$. The functions f_i and g_i depend on the states, controls and some of the state derivatives. These expressions are calculated using MATLAB Symbolic Toolbox in order to avoid potential computation errors.

Continuing with the dynamic inversion process, Eq. (36) can be used to compute the control inputs:

$$\begin{bmatrix} q_c \\ r_c \end{bmatrix} = \begin{bmatrix} g_{11} & g_{12} \\ g_{21} & g_{22} \end{bmatrix}^{-1} \begin{bmatrix} \dot{n}_{z,d} - f_{11} \\ \dot{n}_{y,d} - f_{22} \end{bmatrix} \tag{37}$$

where $\dot{n}_{i,d}$ represent the desired dynamics. The matrix composed of the terms g_{ij} is square (equal number of inputs and outputs) and is easily invertible. This inversion allows for us to efficiently decouple and also linearize the projectile dynamics. Applying the control laws in Eq. (37), the original system is reduced to two decoupled systems, being each one represented by a single integrator:

$$\begin{bmatrix} \dot{y_1} \\ \dot{y_2} \end{bmatrix} = \begin{bmatrix} \dot{n}_z \\ \dot{n}_y \end{bmatrix} = \begin{bmatrix} \dot{n}_{z,d} \\ \dot{n}_{y,d} \end{bmatrix} \tag{38}$$

The same controller applied to both pitch-yaw channels needs to be designed since the projectile aerodynamic properties are (almost) symmetric. By considering an ideal inversion, the control structure in Fig. 4 is proposed in order to impose the desired closed-loop dynamics. This structure is known as 2-DOF controller since it adds a feedforward control to the commanded signal and helps to improve the transient response at high frequencies. Selecting the gains in Fig. 4 as $f_c = 0.5$ and $f_i = 0.25$, the closed-loop response will depend only on the gain K_b, thus resulting in a simple first order system (Ducard (2009)):

$$\frac{y_m}{y_c} = \frac{K_b/2}{s + K_b/2} = \frac{1}{\tau s + 1} \tag{39}$$

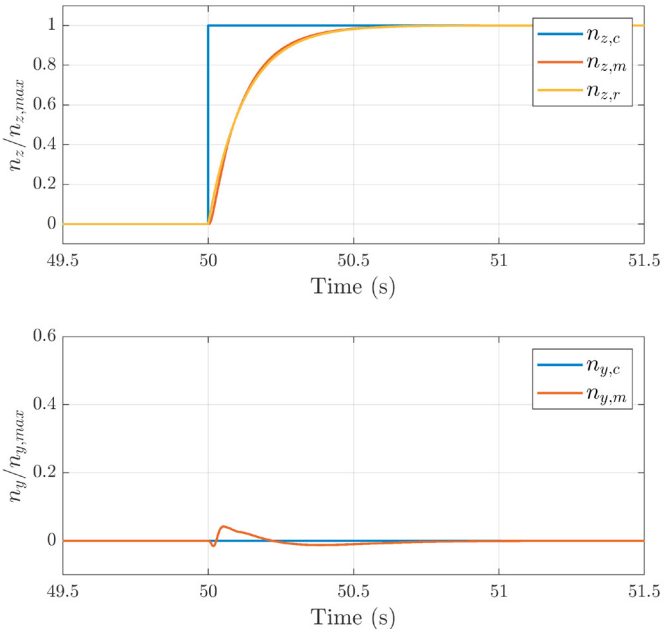

Fig. 5. Closed-loop load factor step response.

The time constant is selected as $\tau = 0.125$ resulting in a settling time around $t_s = 0.5$s Hence, the gain of the controller is computed as $K_b = 16$.

The closed-loop step response as obtained from the nonlinear simulator is shown in (see Fig. 5). From this figure it can be observed how the projectile is able to successfully track the commanded normal acceleration. It is also important to note that the NDI controller is able to decouple quite satisfactorily the pitch from the yaw dynamics since the coupling effects are quickly attenuated. Furthermore, it can be observed that the normal acceleration presents a response almost like the reference model. There is a small delay at the beginning but this was expected due to actuator dynamics being neglected in the design phase.

4. SIMULATION RESULTS

This section presents the results obtained for a fully guided flight, allowing us to assess the effectiveness of the controllers proposed.

The projectile flight trajectory can be divided into two parts: a ballistic and a guided phase (see Fig. 6). During the ballistic phase ($0 \leq t < t_{guid}$), the projectile is launched and all required actions to prepare the projectile for the guided phase are carried out. Due to the harsh initial conditions, during the interval ($0 \leq t < t_{start}$) the electronic components are switched off to avoid any possible damage. Once the projectile transients have settled down, the electronic components are activated at t_{start}, and a new sub-phase can be established between ($t_{start} \leq t < t_{switch}$). During this part of the ballistic flight, the objective is to reduce the fuze roll rate being quite high due to the friction between the main body and the fuze. Once the fuze roll rate is small enough, at t_{switch} the roll autopilot is enabled and sets a determined roll angle for the fuze. This sub-phase is defined between ($t_{switch} \leq t < t_{guid}$). Finally at t_{guid}, the guidance module is activated and the lateral autopilot starts to work.

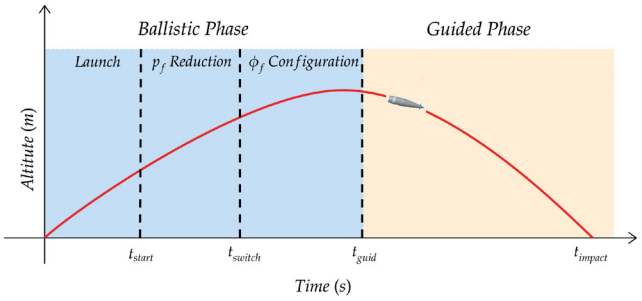

Fig. 6. Projectile flight trajectory.

During the guided phase lasting until the impact point ($t_{guid} \leq t < t_{impact}$), all required corrections provided by the guidance laws have to be computed by the autopilot.

The nonlinear simulation results assuming nominal initial conditions and no system uncertainties are given in Figures 7 and 8. The ballistic phase is illustrated in Fig. 7, where the fuze roll angle, the angular rate and the control deflection are shown. During the ballistic phase, before starting the roll control it is necessary to decrease the fuze rate p_f (see Fig. 7b). This can be done setting a constant deflection $\delta_p = 10$ deg, at $t_{start} = 20$ s. Once the rate is reduced enough to a threshold $p_f = 10\pi$ rad/s, the roll control is activated. Finally, the fuze angle is maintained by the roll autopilot to $\phi_f = 0$ deg, and this configuration is maintained during the whole guided phase.

The lateral guided phase is shown in Fig. 8, starting at $t_{guid} = 30$ s. It shows the load factors for the pitch/yaw channels and the control deflection angles and rates. During this phase, the tracking performance of the load factors is very tight, achieving a good precision at the impact point (see Fig. 8a). Furthermore, the control deflections shown in Fig. 8b are rather small along the flight trajectory, allowing for a large margin until actuator position saturation. In terms of rate deflections, despite the large values at the beginning of the guidance, these remain at a small value for most of the simulation (see Fig. 8c).

NDI is known to being dependent on an accurate system model, however the proposed TSS approach still provides with a certain robustness margin (see Menon et al. (1997)). The system robustness was assessed by a Monte Carlo simulation considering uncertainties on the aerodynamic coefficients (totally 300 cases).

5. CONCLUSION & FUTURE WORK

In this paper, a nonlinear autopilot for a 155mm dual-spin guided projectile was designed in order to deal with its highly nonlinear and strongly coupled dynamics. The roll channel autopilot was first designed according to NDI control theory using an input-output feedback linearization method. The linear controller used to set the desired closed-loop dynamics was tuned based on simple settling time and overshoot requirements. The lateral autopilot design relies also on NDI-based control and a Time Scale Separation (TSS) approach by distinguishing between two time-scales. Both the inner (faster) and the outer (slower) system dynamics were linearized and a linear controller was similarly designed for each resulting system based also on settling time and overshoot requirements.

All controllers were evaluated using a guided flight nonlinear simulation for nominal and uncertain conditions and the results showed satisfactory tracking performance and impact precision. Future work will focus on theoretically assessing the system robustness under the TSS approach. Furthermore, observers need to be added to access certain system states necessary for the NDI-based controller.

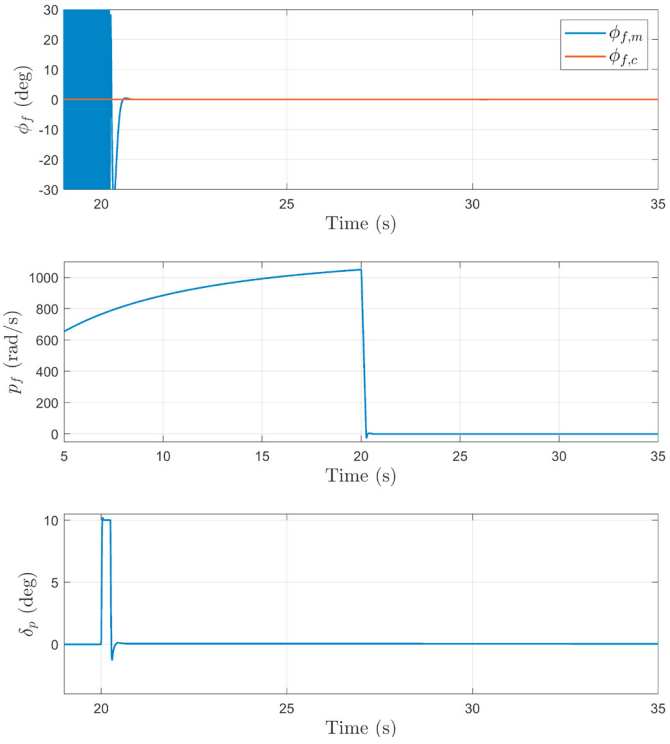

Fig. 7. Nominal simulations: (a) nose roll angle, (b) nose roll rate, (c) roll deflection angle.

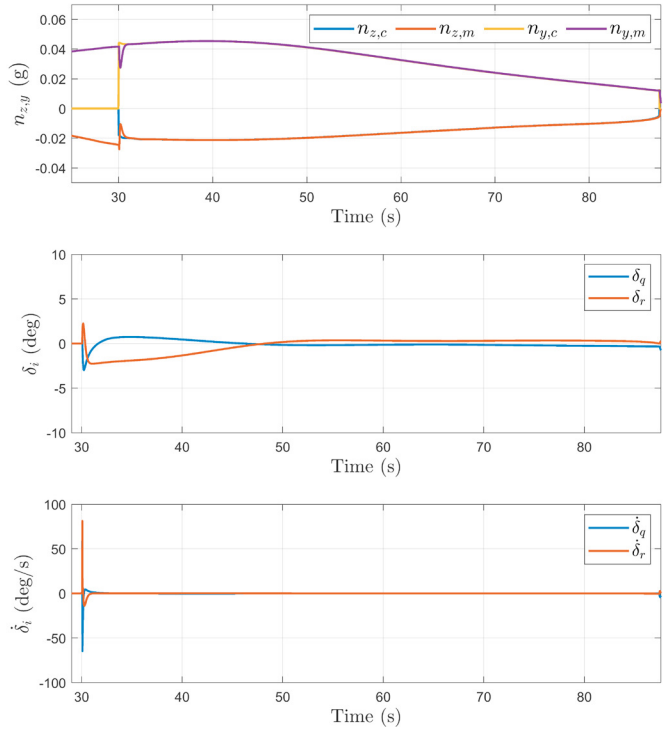

Fig. 8. Nominal simulations: (a) pitch/yaw load factors, (b) deflection angles, (c) deflection angle rates.

REFERENCES

Costello, M. and Peterson, A. (2000). Linear theory of a dual-spin projectile in atmospheric flight. *Journal of Guidance, Control, and Dynamics*, 23(5), 789–797.

da Costa, R.R., Chu, Q.P., and Mulder, J.A. (2003). Reentry flight controller design using nonlinear dynamic inversion. *Journal of Spacecraft and Rockets*, 40(1).

Davis, B., Malejko, G., Dohrn, R., Owens, S., Harkins, T., and Bischer, G. (2009). Addressing the challenges of a thruster-based precision guided mortar munition with the use of embedded telemetry instrumentation. Technical report, ARL Aberdeen Proving Ground.

Ducard, G.J. (2009). *Fault-tolerant flight control and guidance systems: Practical methods for small unmanned aerial vehicles*. Springer Science & Business Media.

Fresconi, F., Celmins, I., and Fairfax, L. (2012). Optimal parameters for maneuverability of affordable precision munitions. In *50th AIAA Aerospace Sciences Meeting*.

Lee, H., Lee, C.H., and Jun, B.E. (2014). Autopilot design for dual-spin projectile based on pi and feedback linearization control. In *2014 IEEE Conference on Control Applications (CCA)*, 2084–2088. IEEE.

Menon, P., Iragavarapu, V., Ohlmeyer, E., Menon, P., Iragavarapu, V., and Ohlmeyer, E. (1997). Nonlinear missile autopilot design using time-scale separation. In *Guidance, Navigation, and Control Conference*, 3765.

Menon, P. and Yousefpor, M. (1996). Design of nonlinear autopilots for high angle of attack missiles. In *Guidance, Navigation, and Control Conference*, 3913.

Sève, F., Theodoulis, S., Wernert, P., Zasadzinski, M., and Boutayeb, M. (2017a). Flight dynamics modeling of dual-spin guided projectiles. *IEEE Transactions on Aerospace and Electronic Systems*, 53(4), 1625–1641.

Sève, F., Theodoulis, S., Wernert, P., Zasadzinski, M., and Boutayeb, M. (2017b). Gain-scheduled h infinity loop-shaping autopilot design for spin-stabilized canard-guided projectiles. *Aerospacelab Journal*.

Sung, J., Kim, B.S., and Song, M.S. (2019). Neural network-based adaptive control design of dual-spin projectile with rotating canards. *International Journal of Aeronautical and Space Sciences*, 20(3), 806–814.

Theodoulis, S., Gassmann, V., Wernert, P., Dritsas, L., Kitsios, I., and Tzes, A. (2013). Guidance and control design for a class of spin-stabilized fin-controlled projectiles. *Journal of Guidance, Control, and Dynamics*, 36(2), 517–531.

Theodoulis, S., Sève, F., and Wernert, P. (2015). Robust gain-scheduled autopilot design for spin-stabilized projectiles with a course-correction fuze. *Aerospace Science and Technology*, 42, 477–489.

Theodoulis, S. and Wernert, P. (2017). Flight dynamics & control for smart munition: The isl contribution. *IFAC-PapersOnLine*, 50(1), 15512–15517.

Wernert, P., Theodoulis, S., and Morel, Y. (2010). Flight dynamics properties of 155 mm spin-stabilized projectiles analyzed in different body frames. In *AIAA atmospheric flight mechanics conference*, 7640.

Yuanchuan, S., Jianqiao, Y., Guanchen, L., Xiaolin, A., Zhenyue, J., and Fangzheng, C. (2017). Observer-based adaptive sliding mode backstepping output-feedback dsc for spin-stabilized canard-controlled projectiles. *Chinese Journal of Aeronautics*, 30(3), 1115–1126.